DNA Binding of Tilorone: ^{1}H NMR and Calorimetric Studies of the Intercalation

Tomoki Nishimura,§ Tadashi Okobira,§ Andrew M. Kelly,‡ Naohiko Shimada,§ Yoichi Takeda,§ and Kazuo Sakurai*,§

Department of Chemical Processes & Environments, The University of Kitakyushu, 1-1 Hibikino, Wakamatsu-ku, Kitakyushu, Fukuoka 808-0135, Japan, and Department of Chemistry, University of Bath, Bath, BA2 7AY, U.K.

Received November 21, 2006; Revised Manuscript Received May 8, 2007

ABSTRACT: The fluorene derivative tilorone has received great attention as a DNA intercalator and has been widely recognized as an inducer of interferon. The biological activity of tilorone is known to be related to its binding mode with DNA; however, few structural and thermodynamic studies have elaborated on this issue. This paper presents two-dimensional (2-D) NMR and isothermal titration calorimetry (ITC) for the tilorone/DNA complex, coupled with circular dichroism (CD) spectroscopy and viscosity measurements. NMR investigation suggests that tilorone binds to DNA through intercalation, showing greater affinity for insertion between AT base pairs than between CG pairs. CD spectral changes were observed for T/B (tilorone/DNA base pair molar ratio) ratios greater than the stoichiometric ratio generally expected for intercalators (i.e., T/B = 0.5, according to the neighbor-exclusion principle). However, there was a clear plateau in the CD intensity between T/B < 0.35 and T/B > 0.45. From comparison with NMR and other measurements, we postulate that CD changes below the plateau should be related to the intercalation and the latter to electrostatic interactions and nonspecific bindings. ITC data showed that $\Delta H < -T\Delta S < 0$, which indicated that tilorone/DNA binding is enthalpy controlled. The magnitude of K_b (the binding constant) was of the same order as that of ethidium bromide. The stoichiometric number, obtained from ITC, CD, and UV data, implied a relatively smaller value (0.28−0.35) than that of the neighbor-exclusion principle. This is because side chains located in the groove disrupt further intercalation to the adjacent sites.

Intercalation is a term used in host−guest chemistry for the reversible inclusion of a molecule (or group) between two other molecules (or groups). In recent years, the intercalation of molecules between the base pairs of DNA has received great interest, notably in the chemotherapeutic inhibition of DNA replication in rapidly growing cancer cells (*1*, *2*). Upon intercalation, the conformation of the DNA backbone is dramatically affected, generally becoming more "rodlike" due to increasing chain stiffness (*3*), and produces new circular dichroism (CD) and UV spectra due to quantum−chemical interactions between the bases and the intercalators. An apparent essential structural feature of such intercalators is the inclusion of planar, extensively delocalized heteroaromatic rings, typically comprising three fused six-membered rings. The most widely utilized intercalator in biological assays, ethidium bromide (EtBr), itself comprising of a phenanthridine core, displays a loss of optical density (hypochromicity) as well as a dramatic increase in fluorescence intensity following intercalation between two base pairs of DNA (*4*). The maximum number of intercalators that can bind to DNA helices is one intercalator versus two base pairs. This "neighbor-exclusion principle" is one of the characteristic features of DNA intercalators (*5*).

Fluorene is a tricyclic aromatic hydrocarbon comprising two phenolic aromatic rings fused to either side of a five-membered ring. Fluorene seems therefore to perfectly possess the structural requirements for DNA intercalation. There have been several studies of fluorene derivatives, including tilorone-derived (2,7-bis[(diethylamino)-ethoxy]-fluoren-9-one, Figure 1) (*2*, *6*), 9-fluoren-β-*O*-glycosidem (*7*), and 2,7-bis-[(dialkylamino)-acetylamino]-fluoren-9-one derivatives (fluoramides) (*6*). Tilorone has been widely studied since it has been reported to induce interferon (*8*). Understanding the DNA binding of tilorone is essential for understanding the mode of biological action and for the development of superior synthetic derivatives. To this end, there has been little work to examine tilorone binding to DNA from structural and thermodynamic stand points.

Bischoff et al. synthesized several fluoramide derivatives and studied their DNA binding with CD and surface plasmon resonance (SPR), relative to tilorone (*6*). The CD signals were dramatically affected on addition of the fluoramides (or tilorone) to the DNA. The CD changes did not reach saturation, even when the mixing ratio exceeded the ratio expected from the neighbor-exclusion principle. The lack of an upper limit for the ratio of tilorone/DNA interaction was confirmed with SPR. They ascribed this abnormal feature to multiple interaction modes including intercalation and groove-binding based on the AMBER molecular modeling. This work posed various questions, such as what is the major binding mode, the cause of no apparent upper limit of the tilorone/DNA interacting ratio, and what are the accurate thermodynamic values of the binding constant, the entropy and enthalpy changes.

* Corresponding author. E-mail: sakurai@env.kitakyu-u.ac.jp. Fax: +81-93-695-3390. Phone: +81-93-695-3298.
§ The University of Kitakyushu.
‡ University of Bath.

10.1021/bi602402m CCC: $37.00
Published on Web 06/16/2007

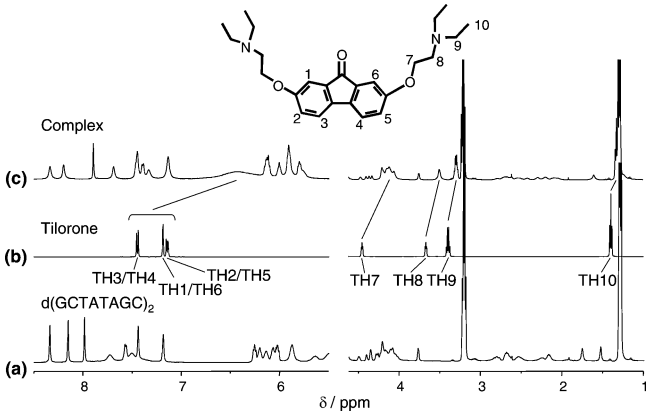

FIGURE 1: ^{1}H NMR spectra (500 MHz) showing (a) the proton signals from naked d(GCTATAGC)$_2$, (b) the aromatic proton signals H1−H6 of tilorone (left) and the side chain protons signals H7−H10, and (c) characteristic chemical shift changes in the 2:1 DNA−drug complex. All spectra were taken at 313 K in 99.996% D_2O, 10 mM phosphate buffer, and 25 mM NaCl.

This paper presents conclusions to these fundamental questions.

EXPERIMENTAL PROCEDURES

Materials. Tilorone was obtained from Wako (Japan) and used without further purification. Sonicated salmon sperm DNA (sss-DNA)[1] was purchased from Amersham biosciences (Japan). DNA sequence GCTATAGC was synthesized and purified using HPLC at GENENET (Japan). Double-stranded DNA d(GCTATAGC)$_2$ was annealed by slow cooling from 90 °C to room temperature. The terminating GC base pair of d(GCTATAGC)$_2$ is expected to enhance the thermal stability and reduce end-dissociation of the duplexes in NMR experiments performed at elevated temperatures.

Intercalation. Tilorone (5.0 mg) was dissolved in 1.0 mL of dimethyl sulfoxide (DMSO), and the resultant tilorone/DMSO solution was added to an appropriate amount of DNA aqueous solution (30 μM, 10 mM Tris-HCl, and 1 mM NaCl). The DMSO concentration after mixing was 1.0 vol %. Hereafter, the molar ratio of tilorone to the DNA base pair is denoted by T/B.

One- and Two-Dimensional ^{1}H NMR. NMR spectra were measured at 500 MHz on a JNM-ECP500 spectrometer at 313 K. An oligomer concentration of 34.2 mM (in base pairs) was used, and the melting temperature (ca. 325 K, see Figure S6, Supporting Information) of the DNA at this concentration is higher than the measurement temperature. The chemical shifts (ppm) were referenced to internal 3-(trimethylsilyl)-1-propanesulfonic acid sodium salt, DSS. One-dimensional (1-D) ^{1}H NMR spectra were recorded with a total of 16.4 k data points, 64 transients, and a recycle delay of 4 s. Two-dimensional (2-D) NMR data sets were acquired with 2048 complex points in t_2, 512 points in t_1, and 32 transients with a recycle delay of 1.5 s. 2-D NOESY (nuclear overhauser effect spectroscopy) spectra were acquired with 2048 complex points in t_2, 256 points in t_1, 64 transients per t_1 increment, and a recycle delay of 2 s. The mixing times were 250, 350, and 450 ms. All data were multiplied with optimized phase-shifted squared sinebell apodization functions and zero-filled to a final matrix of 2048 × 2048 data points before Fourier transformation.

Viscosity Measurements. Viscosity measurements were carried out according to the established method (*9*) to determine the intrinsic viscosity [η] as a function of T/B for sss-DNA solutions at 25.0 °C through use of an Ubbelohde type viscometer immersed in a 25.0 °C water bath. [η] is related to the solution viscosity (η) by the eqs 1 and 2.

$$\eta_{in} = \frac{\ln(\eta/\eta_{sol})}{c\eta_{sol}} \quad (1)$$

$$[\eta] = \lim_{c\to 0}(\eta_{in}) \quad (2)$$

Here, η_{sol} and c represent the solvent viscosity and the concentration of DNA, respectively. The relationship between [η] and T/B was obtained in a buffer solution (10 mM Tris-HCl , 1 mM NaCl, and 1% DMSO) at pH 7.5. sss-DNA samples were dialyzed with extra-pure water for 24 h and lyophilized before the measurements. As presented in Supporting Information, we confirmed that this salt concentration does not cause up-turn of the solution viscosity at dilute polymer concentrations owing to the intramolecular electrostatic repulsion, and thus the extrapolation in eq 2 was performed successfully.

CD and UV Spectroscopy. CD and UV spectroscopy were measured with a Jasco J-720WI spectropolarimeter with a 1.0 cm cell and a Jasco V-570 spectrophotometer, respectively. The experimental procedures are detailed elsewhere (*10*).

Isothermal Titration Calorimetry (ITC). Heat flow during isothermal titration was measured with a VP-ITC MicroCal microcalorimeter (Northampton, MA). Titration data were processed with the software provided by the manufacturer (*11*). DNA (0.2 mM) was maintained in the sample cell (1.4301 mL) at 25 °C in 10 mM Tris-HCl (pH 7.5), 1% DMSO, and the whole cell was stirred at 300 rpm. A tilorone solution (2.0 mM) was introduced into the sample cell by means of a syringe via 25 individual injections [each injection was 7 μL containing tilorone (9.7 μM) in 10 mM Tris-HCl-(pH 7.5), 1% DMSO]. Injections were 14 s in duration, and individual injections were programmed at intervals of 250 s. The injection intervals, the volume of the injectant, and the number of injections have been adjusted such that the binding is completed toward the end of the titration. After the peak area was integrated and the heats of dilution were subtracted, the thermogram for the binding was obtained. The titration data was processed with the software provided by the manufacturer and fit using a two (or one) binding sites model (*12*) using nonlinear least-squares analysis to determine the enthalpy (ΔH), entropy (ΔS), binding constant (K_b) for the binding, and drug/base pair stoichiometry (n).

In Vitro Transcription/Translation Assay. An in vitro cell-free transcription/translation assay was carried out using GFP expression plasmid DNA, pQBI 63 (Takara), in the *Escherichia coli* T7 S30 extract system (Promega). The pQBI 63 was amplified using *E. coli* BL21(DE3) (Novagen) and

[1] Symbols and abbreviations: sss-DNA: sonicated salmon sperm DNA; T/B: molar ratio of tilorone to the DNA base pair; [η]: intrinsic viscosity; CD: circular dichroism; ITC: isothermal titration calorimetry; ΔH: enthalpy change; ΔS: entropy change; K_b: binding constant; n: drug/base pair stoichiometry; GFP: green florescence protein.

Table 1: Chemical Shift Change $\Delta\delta$ Values (ppm) of Tilorone

sample	H1/H6	H2/H5	H3/H4	H7	H8	H9	H10
tilorone alone	7.191	7.155	7.457	4.464	3.679	3.419	1.413
complex		6.420 (6.75−6.00)		4.121	3.506	3.320	1.345
$\Delta\delta$	−0.441 to −1.191	−0.405 to −1.155	−0.707 to −1.457	−0.343	−0.173	−0.099	−0.068

Table 2: Chemical Shift Change $\Delta\delta$ Values (ppm) of $d(GCTATAGC)_2$

proton	sample	T3	A4	T5	A6
		Major Groove Protons			
H8/H6	DNA alone	7.439	8.338	7.185	8.153
	complex	7.449	8.338	7.135	8.199
	$\Delta\delta$	0.010	0	−0.050	0.046
CH_3	DNA alone	1.754		1.526	
	complex	1.608		1.230	
	$\Delta\delta$	−0.146		−0.296	
H2′/H2″	DNA alone	2.683/2.777	2.683/2.807	2.243	2.683/2.807
	complex	2.296	2.676/2.788	2.102/2.202	2.694
	$\Delta\delta$	−0.387/−0.481	−0.007/−0.019	−0.141/−0.041	0.011/−0.113
		Minor Groove Protons			
H1′	DNA alone	6.067	6.256	5.638	6.024
	complex	5.908	6.128	5.761	5.908
	$\Delta\delta$	−0.159	−0.128	0.123	−0.116

purified with the Plasmid Midi kit (Qiagen). When 1.38 μg of pQBI 63 was added to 16 μL of *E. coli* extract solution and the solution was incubated at 37 °C, the plasmid DNA produced a sufficient amount of GFP to provide a florescence maximum at 507 nm (excited at 463 nm). We then adopted this protocol as the reference system. We prepared four pQBI 63 samples that had been intercalated with tilorone (T/B = 0.3, 0.5, and 1.0) and EtBr (EtBr/B = 0.5), and the amount of GFP expressed was evaluated in terms of the fluorescence intensity.

RESULTS AND DISCUSSION

Structural Studies with NMR. Standard 2-D NOESY and COSY spectroscopic analysis was applied to assign the nonexchangeable protons of tilorone and $d(GCTATAGC)_2$. The assignments and the chemical shifts are summarized for tilorone (Table 1) and $d(GCTATAGC)_2$ (Table S1, Supporting Information). The assignment of the base and deoxyribose protons were accomplished using both H1′(i-1) → H8/H6(i) and H2′/H2″(i-1) → H8/H6(i) sequential NOE contacts. Figure 1 compares ^{1}H NMR spectra before and after addition of tilorone to $d(GCTATAGC)_2$ (2:1 molar ratio). The tilorone resonances all showed an upfield shift upon mixing. The chemical shift changes ($\Delta\delta$) are listed in Table 1. Upon mixing, *N*-ethyl resonances TH10 and TH9 show an upfield shift of 0.068 and 0.099 ppm, respectively. Much larger shifts are observed for the six fluorene aromatic protons TH1−TH6 (0.4−1.5 ppm). Also worthy of note is that all peaks for both the DNA and tilorone broadened significantly, particularly the tilorone aromatic protons TH1−TH6.

This upfield shift of TH1−TH6 indicates that the fluorene moiety is shielded by the ring current magnetic field generated by DNA base moieties. This is as expected if the fluorene moiety is closely located in parallel to the DNA bases, presumably intercalating between DNA base pairs. Generally, the magnitude of $\Delta\delta$ depends on the relative positioning of the guest molecule between the DNA bases. In our case, however, we could not specify which tilorone aromatic portion penetrated deeply (or shallowly) into the base stack because of the coalescence of the TH1−TH6 peaks. The peak broadening is likely due to both the slower tumbling of the complex relative to the tilorone and the reversible exchange of tilorone between DNA and solution.

Baruah and Bierbach (*13*) recently reported the NMR investigation of an acridine derived intercalating complex: 1-[2-(acridin-9-ylamino)ethyl]-1,3-dimethylthiourea. They suggested that penetration of the duplexes occurred from the minor groove. They observed pronounced upfield shifts of 0.5−1.0 ppm of the acridine aromatic protons. The degree of shift was in the same range as that of the tilorone/DNA binding, while the peak broadening of the acridine aromatic protons was much less than that of the intercalated tilorone.

2-D NOESY spectroscopy of the complex did not show any NOE correlation between the tilorone aromatic protons and the DNA protons because of the broadened aromatic peaks of the intercalated tilorone. This proved a considerable disadvantage for structural analysis, although 2-D NOESY data showed clear disruption of the sequential NOE connectivity of DNA. A section of the 2-D NOESY spectrum is depicted in Figure 2. No NOE correlation was observed between A4H8 and T3CH_3 and between A6H8 and T5H1′ as indicated by the solid lines and arrows in the Figure 2. These correlations were clearly present prior to mixing. By contrast, strong internucleotide cross-peaks were observed between the A4 and T5 bases, for example, between A4H1′ and T5H6 presented with the dotted line. From this, we conclude that tilorone intercalates into the 5′-T3A4/A6T5 base step as presented by the schematic in Figure 2. The AT sequence specificity for the tilorone intercalation was consistent with the results of calorimetric titration (see Table 4, K_b for AT is almost 10 times larger than that of GC). It is interesting that there was no evidence for tilorone intercalation into the A4T5/T5A4 base step. We postulated that this was due to the experimental conditions, wherein the molar ratio of tilorone to total AT base pair was 2:3. In this composition, if tilorone intercalates into A4T5/T5A4, the adjacent T3A4/A6T5 pair should be excluded from the next possible binding site due to the neighbor-exclusion

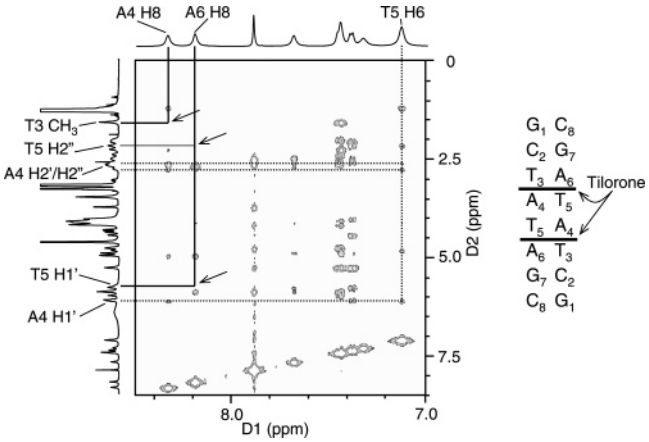

FIGURE 2: 2-D NOESY of the tilorone/d(GCTATAGC)$_2$ complex obtained at 500 MHz and 313 K. The dotted lines show sequential connectivity between A4H1′ and T5H6. Absent cross-peaks due to disruption of the A4H8-T3CH$_3$ and A6H8-T5H1′ are indicated by arrows on the solid lines. The right side schematics show how two tilorone molecules intercalate into d(GCTATAGC)$_2$.

principle, and the remaining tilorone then intercalates between the AT and CG base pairs. This situation is more thermodynamically unfavorable than two tilorone molecules binding to both T3A4/A6T5 and A6T5/T3A4 pairs.

The cationic tertiary amine of the tilorone side chain should bind to the phosphate anion of DNA after the fluorene portion is intercalated (Figure S7, Supporting Information). In fact, when we carried out molecular modeling, the distance between the amine and phosphate groups was found to be short enough for interaction. The question is whether the ethylene linker, connecting the fluorene to amine moieties, locates in the major or minor groove. In the major groove, H6/H8, TCH$_3$ and ribose H2′/H2″ protons are present. These protons, called "major groove protons", are sensitive to the presence of guest molecules. In particular, TCH$_3$ protons stick out in the major groove and are thus very sensitive to guest molecules. Likewise, ribose H4′, H1′, and AH2 protons are known as "minor groove protons". Table 2 presents how these protons are shifted upon intercalation. The most significant change in chemical shift of −0.15 to −0.30 ppm was observed for the major groove protons of T3CH$_3$ and T5CH$_3$. However, minor groove protons such as H1′ also shifted. Unfortunately, it is not clear from the present NMR data which groove the tilorone side chains bind in. They could bind in either groove.

Intrinsic Viscosity and Electrophoretic Migration. Figure 3 plots [η] against T/B. [η] increased with increasing T/B and reached a value larger than that of untreated DNA by 28% at T/B = 0.7. The increment of [η] should be ascribed to the increment of hydrodynamic volume owing to increased stiffness of DNA. This feature is consistent with the fact that tilorone is an intercalator (*14*). As mentioned previously, the maximum number of intercalators that can bind to DNA is one intercalator versus two base pairs (neighbor-exclusion principle), i.e., T/B = 0.5. As presented in Figure 3, [η] kept increasing above this composition, a result that is consistent with Bischoff et al. (*6*). At T/B = 1.0, [η] = 4.4 × 10^2 cm^3 g^{-1}, smaller than that of T/B = 0.7. We presume that this viscosity drop at relatively higher T/B can be ascribed to the compaction of the DNA conformation. The higher T/B ratio effect is discussed in more detailed in the CD section.

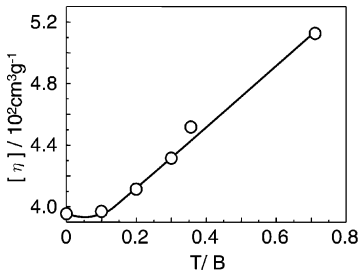

FIGURE 3: T/B dependence of the intrinsic viscosity [η] of sss-DNA in a Tris buffer (10 mM Tris-HCl, 1 mM NaCl, and 1% DMSO) at pH 7.5. The salt concentration was chosen so that there was no up-turn of the solution viscosity at dilute polymer concentrations owing to the intramolecular electrostatic repulsion.

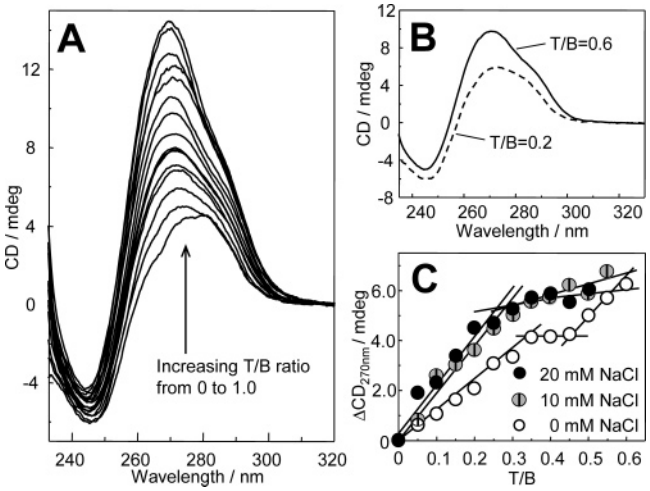

FIGURE 4: (A) CD spectral changes when T/B was increased from 0 to 1, (B) comparison of the CD spectra between T/B = 0.2 and T/B = 0.6, where the T/B = 0.2 spectrum was multiplied by a factor of 1.65, (C) the difference of the CD intensity at 270 nm ($\Delta CD_{270\ nm}$) plotted against T/B for three different NaCl concentrations.

Geller et al. (*2*) investigated the T/B dependence of the relative viscosity and reported that the viscosity increment was saturated at approximately T/B = 0.2. We did not observe the viscosity saturation at such a low T/B, and the reason for this discrepancy is not clear. As presented in Supporting Information, the polyelectrolyte effect (i.e., up-turn of the relative viscosity at low concentrations) was suppressed at [NaCl] > 1.0 mM, and thus the extrapolation to the infinitely diluted state was successfully carried out in our case. In this sense, the discussion based on [η] should be more accurate than that of the relative viscosity.

Changes in the hydrodynamic volume should reflect the gel electrophoretic migration (*15*). The gel mobility shift experiments were virtually unaffected by the presence of tilorone (data not shown). The gel electrophoresis data seemed to contradict that of viscometry. We presumed that when the electric field was applied in the gel, the positively charged tilorone might dissociate from the anionic DNA and they migrate to opposing terminals. This observation suggests that either the binding constant between tilorone and DNA is relatively low or the activation energy for binding is smaller than conventional intercalators.

Spectroscopic Studies with CD and UV. Figure 4A presents the CD changes when T/B was incremented from 0 to 1.0. As remarked upon by Bischoff et al. (*16*), the CD change

Table 3: Thermodynamic Parameters for the Association of Tilorone with sss-DNA at Different Salt Concentrations

$[Na^+]$/mM	ΔH/kcal mol^{-1}	$T\Delta S$/kcal mol^{-1}	ΔG/kcal mol^{-1}	$K_b \times 10^5$/M^{-1}	n
0	-6.65 ± 0.33	0.61	-7.24 ± 0.70	2.08 ± 0.31	0.288 ± 0.01
5	-6.45 ± 0.35	0.65	-7.09 ± 0.93	1.61 ± 0.21	0.291 ± 0.02
10	-6.50 ± 0.26	0.65	-7.14 ± 1.04	1.77 ± 0.17	0.287 ± 0.01
15	-6.32 ± 0.09	0.77	-7.07 ± 1.35	1.56 ± 0.10	0.297 ± 0.01
20	-6.07 ± 0.15	0.91	-6.97 ± 0.09	1.32 ± 1.16	0.316 ± 0.21
25	-5.86 ± 0.10	1.08	-6.92 ± 0.05	1.22 ± 0.93	0.350 ± 0.00
30	-5.43 ± 0.10	1.39	-6.81 ± 1.53	1.01 ± 0.07	0.356 ± 0.01

Table 4: Thermodynamic Parameters for the Association of Tiorone with poly(dA-dT) and poly(dC-dG) at [NaCl] = 25 mM

DNA	ΔH/kcal mol^{-1}	$T\Delta S$/kcal mol^{-1}	ΔG/kcal mol^{-1}	$K_b \times 10^5$/M^{-1}	n
poly(dA-dT)	-5.03 ± 0.20	3.13	-8.14 ± 0.20	9.54 ± 3.66	0.141 ± 0.03
poly(dC-dG)	-3.59 ± 0.07	3.43	-7.00 ± 0.07	1.37 ± 0.12	0.332 ± 0.01

never became saturated even when T/B exceeded the mixing ratio expected from the neighbor-exclusion principle (i.e., T/B = 0.5). When we carefully compared the CD spectra above and below this ratio, there was a subtle but appreciable difference as presented in Figure 4B. At 247 nm, T/B = 0.2 is lower than the corresponding T/B = 0.6, which itself displays a small "shoulder" around 290 nm. A plot of the CD values at 270 nm against T/B (Figure 4C, unfilled circles) showed a flat region in the range of T/B = 0.35−0.45 where the CD bands were essentially identical separating two regions where the binding mode seems different: T/B < 0.35 and T/B > 0.45. When T/B exceeded about 0.8, the CD band gradually collapsed and disappeared (data not shown).

Since NMR data taken at T/B = 0.3 showed that tilorone intercalates into DNA, the CD band at the lower T/B region should be related to the conformational changes upon the intercalation. The intercalation seems to stop around T/B = 0.35, suggesting that the saturating ratio for the tilorone intercalation is less than that of the neighbor-exclusion principle. A similar observation is noted when intercalators have relatively long side chains. Modukuru et al. (*17*) showed that an anthracene derivative bearing a long 1,8-octyldiamine side chain (Table S4 in Supporting Information) has a smaller stoichiometric value than the neighbor-exclusion principle. They argued that the long side chain fits into the minor groove, and thus the binding to the neighboring base pair is obstructed. The same explanation may hold for tilorone since the tilorone side chains are considered to bind to the groove (see the NMR section).

Bischoff et al. (*16*) ascribed the lack of an upper limit of the tilorone binding to the presence of multiple binding modes such as intercalation and groove-binding. Growth of the CD intensity above T/B = 0.45 should be ascribed to bindings other than intercalation. On the other hand, it should be noticed that the disappearance of the CD bands and a decease in $[\eta]$ indicate the involvement of nonspecific bindings that lead to collapse of the DNA conformation. We can presume that coincidental development of the second binding and nonspecific bindings take place at the higher T/B region.

Figure 4C compares the CD increment at 270 nm for three different NaCl concentrations. In the range of [NaCl] > 10 mM, there was no further increment in CD in the higher T/B region. This feature suggests that the CD changes in higher T/B are triggered by electrostatic interaction, presumably ion pair formation between DNA anions and tilorone amino cations. Once the ion pairs form, they lose hydrophilicity and sometimes precipitate out of solution. We postulate, therefore, that the disappearance of CD and decrease of $[\eta]$ are correlated to hydrophobic collapse occurring between DNA and tilorone, which are similar to coil−globule transitions (*18*).

The interaction of tilorone with sss-DNA was investigated using absorption spectroscopy (data not shown). Addition of sss-DNA to such solutions resulted in distinctive changes in the UV spectrum of tilorone. Bands at 270 nm showed a high degree of hypochromicity, while the peak maximum was shifted from 270 to 280 nm. This change was consistent with previous work from Zang et al. (*19*). Plot of ΔAbs at 270 nm against T/B showed the upper limit of the UV change (data not shown). The turn-off point indicated T/B = 0.33 is the saturation composition of the intercalation. This value is comparable with the CD data.

Calorimetry To Determine the Thermodynamic Parameters. Figure 5A presents an example of the heat produced during titration of sss-DNA (0.2 mM, [NaCl] = 25 mM) against tilorone. Each addition of the tilorone solution resulted in the release of heat until the binding was saturated. Following integration and background correction, the thermogram for the binding was obtained and presented in Figure 5B.

Figure 5B indicates that the binding is exothermic and that the binding saturates around T/B = 0.6−0.7. The best fits to the data employed a one-site binding model (*12*), and these analyses produced the binding parameters $K_b = 1.22 \times 10^5$ [M^{-1}], $\Delta H = -5.86$ kcal mol^{-1}, $T\Delta S = 1.08$ kcal mol^{-1}, and $n = 0.35$. In the case of [NaCl] < 20 mM, the best fits to the data suggested a two-site binding model (*12*). By analogy with ITC for EtBr binding to DNA (see Supporting Information, Figure S5A and Table S2), the first binding mode can be ascribed to electrostatic interactions, and the second related to intercalation. Figure 5C presents four thermogram curves for different [NaCl] solutions and their best fit curves. In the range of [NaCl] > 25 mM, the contribution from the first mode (electrostatic) became negligibly small, and essentially the data could be fitted with a one-site binding model. The obtained thermodynamic parameters are listed in Tables 3 and S3 (for the first binding), and the results for the second binding have been plotted against [NaCl] in Figure 6.

Figure 6 and Table 3 show that $\Delta H < -T\Delta S < 0$. This feature means that binding is entropically and enthalpically

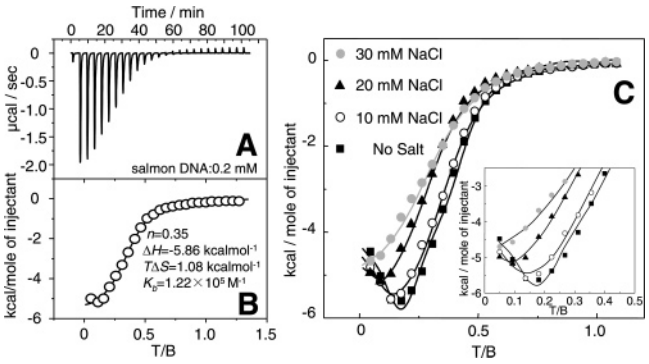

FIGURE 5: Thermodynamic profiles for the ITC measurements. (A) Isothermal calorimetric titration curve obtained when tilorone in 1% DMSO aqueous solution (2.0 mM) was added to sss-DNA (0.2 mM), in equal intervals (250 s) for the initial injection = 1 μL and the other 24 = 7 μL. [NaCl] = 25 mM. (B) Plot of the individual injection heats against T/B and the result of the best-fit curve and resultant parameters. (C) Comparison of the thermogram for four different salt concentrations. The solid lines are the nonlinear least-squares best fit of the data with a two-individual site model.

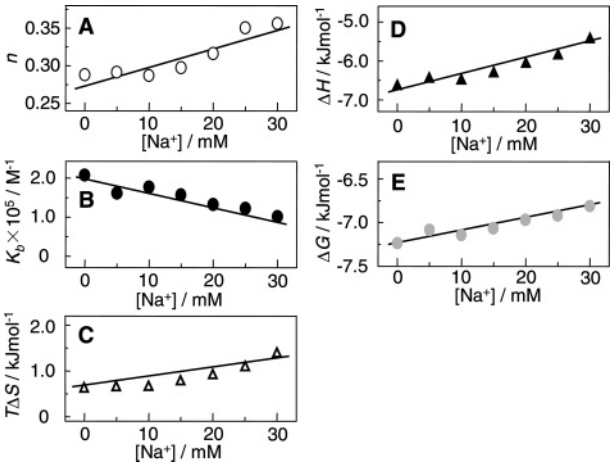

FIGURE 6: (A−E) The salt concentration dependence of the obtained parameters from ITC for the tilorone/sss-DNA interaction.

favorable, while ΔG is mainly influenced by the enthalpy change. This presumably means that electrostatic interactions play a more dominant role than hydrophobic interactions in the tilorone binding, since ΔH and ΔS should be related predominantly to electrostatic interactions and hydrophobic interactions, respectively (*20*). On the other hand, the EtBr system shows $\Delta H < 0 < -T\Delta S$ (see Table S2, Supporting Information), which means that enthalpy is favorable for binding, but entropy is not. This is probably because EtBr has a large phenyl group that can rotate freely in solution and become spatially confined after intercalation, and thus this restricted rotation gives rise to a positive value of $-T\Delta S$. The hydrophobic interactions become more dominant in anthracene derivatives (*17*) and dipyrido[3,2-a:2′,3′-c] phenazine derivatives (*20*) (see Table S4, Supporting Information). By comparison, the $T\Delta S$ term of the tilorone system is small. This could be due to the smaller degree of conjugation relative to that of the anthracene and dipyrido phenazine derivatives lending the tilorone lower hydrophobicity.

Figure 6 shows that K_b decreases with increasing [NaCl]. This is because the magnitudes of both ΔH and $-T\Delta S$ decrease, and both values are negative. Contrary to this system, K_b of EtBr is essentially independent from [NaCl]. The magnitude of K_b of tilorone is in the same range as that of EtBr. The value of n is almost independent of [NaCl] and always less than the value expected from the neighbor-exclusion principle. As mentioned in Figure 4, the smaller n value can be ascribed to the presence of a long side chain.

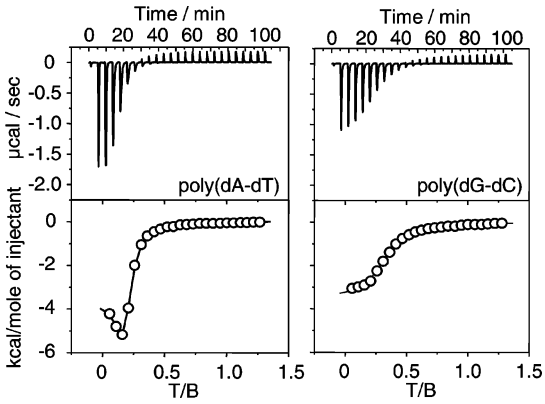

FIGURE 7: ITC thermogram curves for poly(dA-dT) and poly(dG-dC).

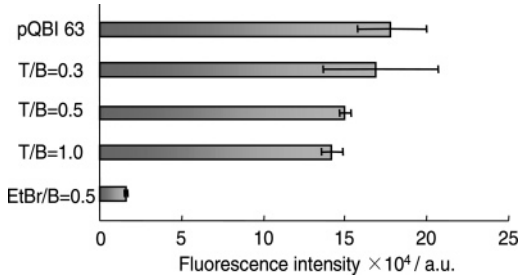

FIGURE 8: In vitro cell-free transcription/translation assay for tilorone-intercalated pQBI 63 in *E. coli* T7 S30 extract solutions. For comparison, the same assay was carried out for EtBr intercalated pQBI 63.

Figure 7 shows the thermogram of poly(dA-dT) and poly(dG-dC) at [NaCl] = 25 mM, and the resultant thermodynamic parameters are listed in Table 4. Being contrary to most other intercalators (*21*, *22*), tilorone shows a larger K_b for poly(dA-dT) than that of poly(dG-dC). This base molecular specificity suggests that the tilorone binding follows the model proposed by Chaires (*23*) where the initial step of the binding is promoted by the separation of DNA base pairs to afford a cavity into which the intercalator can sit. The separation of DNA base pairs is expected to occur more frequently between AT pairs than between GC pairs, and thus the binding to AT is more favorable than GC for the tilorone intercalation.

Protein Expression from Tilorone-Intercalated Plasmid DNA (pDNA). One of the most interesting features of the intercalating fluorene is that proteins can be expressed from the intercalated DNA (*24*, *25*). Figure 8 plots the fluorescence intensity against T/B when a red-shifted green fluorescence protein (GFP) was produced in the cell-free *E. coli* T7 S30 extract solution. With increasing T/B, the fluorescence intensity decreased slightly. Even at T/B = 1.0, the intensity decreased only by 30%. This is quite a contrast to that of EtBr. This difference between two compounds is interesting, considering that both have the same magnitude of K_b. A possible explanation for this is as follows; the activation

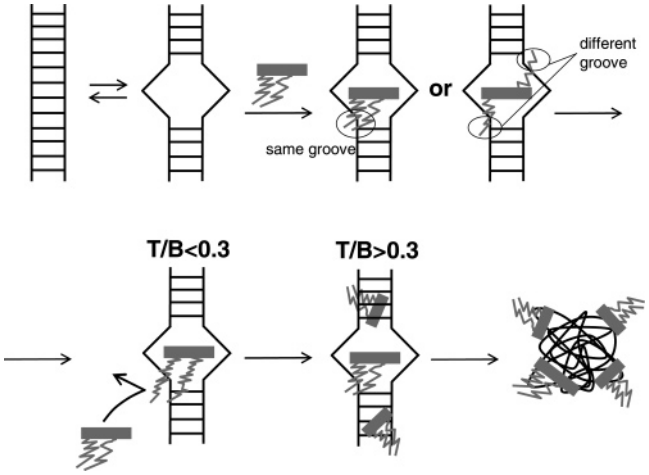

FIGURE 9: Schematic presentation of the tilorone binding mode. In the early stage (T/B < 0.3), tilorone intercalates mainly between AT pairs prepared by separation of the base pair. Once intercalated, the two side chains fit into the groove either both in the same or different grooves. The side chain then disrupts further intercalation to the adjacent site. When T/B increases beyond 0.3, the nonspecific binding driven by electrostatic interaction starts, and this second binding mode never stops until the entire DNA strand collapses.

energy of the tilorone intercalation is smaller than that of EtBr, and thus the dissociation/association can take place more easily in tilorone/DNA than in EtBr/DNA. This speculation is supported by the fact that there was no difference observed in gel electrophoretic pattern for the tilorone-intercalated DNA. Therefore, the facile (or rapid) dissociation/association should allow DNA-binding proteins easy access to the promoter region of DNA and thus carry out the production of mRNA.

Tilorone Binding Model. On the basis of these observations, we can speculate the tilorone binding mode as presented in Figure 9. Initially, tilorone intercalates into the intercalation site that has been prepared by separation of the base pair, mainly AT pairs. This is the reason that we observed the AT pair intercalation predominantly over the GC pairs. In the intercalated state, the two side chains fit into a groove; however, we do not know whether both of them are in the same groove or the tilorone penetrates the base pair so that the side chains are in the different grooves. The side chain disrupts further intercalation to the adjacent site, and thus the stoichiometry of the binding is less than that of the neighbor-exclusion principle. When T/B increases beyond 0.3, the nonspecific binding driven by electrostatic interaction starts, and this second binding mode never stops until the entire DNA strand collapses to lose the CD band and decrease [η].

CONCLUDING REMARKS

The present work shows that tilorone is a DNA intercalator, and the binding constant is of the same magnitude as that of the widely used intercalator EtBr. ITC clarified enthalpy-driven binding. We present our structural and thermodynamic data from which we may draw important conclusions to more fully understand the biological activity of tilorone and to develop new, improved intercalators from tilorone-derived backbones.

ACKNOWLEDGMENT

This work is finanically supported by JST SORST program and Grant-in-Aid for Scientific Research (16350068 & 16655048).

SUPPORTING INFORMATION AVAILABLE

(1) Details of the viscosity measurements, (2) CD spectral changes upon [NaCl] increments, (3) CD for intercalated poly(dA)-poly(dT), poly(dC)-poly(dG), poly(dA-dT), and poly(dC-dG) and the increment of the melting temperature, (4) ITC for EtBr, and other additional numerical data for NMR and ITC, (5) T_m, (6) molecular modeling. This material is available free of charge via the Internet at http://pubs.acs.org.

REFERENCES

1. Wilson, W. D., Wang, Y.-H., Kusuma, S., Chandrasekaran, S., Yang, N., C., and Boykin, D. W. (1985) Binding strength and specificity in DNA interactions: the design of A·T specific intercalators, *J. Am. Chem. Soc. 107*, 4989−4995.
2. Geller, K., Reinert, K. E., and Schulze, W. (1985) Interaction of DNA with tilorone derivatives: viscometric investigations, *Biomed. Biochim. Acta 44*, 1095−1103.
3. Berge, T., Jenkins, N. S., Hopkirk, R. B., Waring, M. J., Edwardson, J. M., and Henderson, R. M. (2002) Structural perturbations in DNA caused by bis-intercalation of ditercalinium visualised by atomic force microscopy, *Nucleic Acids Res 30*, 2980−2986.
4. McMurray, C. T., and Van Holde, K. E. (1991) Binding of ethidium to the nucleosome core particle. 1. Binding and dissociation reactions, *Biochemistry 30*, 5631.
5. Kumar, C. V., and Asuncion, E. H. (1993) DNA binding studies and site selective fluorescence sensitization of an anthryl probe, *J. Am. Chem. Soc. 115*, 8547−8553.
6. Bischoff, G., Gromann, U., Lindau, S., Skolziger, R., Witkowski, W., Bohley, C., Naumann, S., Sagi, J., Meister, W. V., and Hoffmann, S. (2000) A structure-function study of nucleic acid-fluorenone complexes, *J. Biomol. Struct. Dyn. 18*, 199−208.
7. Alcaro, S, Arena, A, Neri, S, Ottanà, R, Ortuso, F, Pavone, B, and Vigorita, M. G. (2003) Design and synthesis of DNA-intercalating 9-fluoren-β-*O*-glycosides as potential IFN-inducers, and antiviral and cytostatic agents, *Bioorg. Med. Chem. 12*, 1781−1791.
8. Krueger, R. F., and Mayer, G. D. (1970) Tilorone hydrochloride: an orally active antiviral agent, *Science 169*, 1213−1214.
9. Stevens, M. P. (1990) *Polymer Chemistry An Introduction*, pp 57−59, Oxford University Press, New York.
10. Wu, Y., S., Koch, K., R., Abratt, V., R., and Klump, H., H. (2005) Intercalation into the DNA double helix and in vivo biological activity of water-soluble planar [Pt(diimine)(*N*,*N*-dihydroxyethyl-*N*′-benzoylthioureato)]+Cl- complexes: A study of their thermal stability, their CD spectra and their gel mobility, *Arch. Biochem. Biophys. 440*, 28−37.
11. ITC Data Analysis in Origin, Tutorial Guide (2004) pp 95−98, Microcal, LLC, Northampton, MA.
12. Breslauer, K. J., Freire, E., and Straume, M. (1992) Calorimetry: a tool for DNA and ligand-DNA studies, *Methods Enzymol. 211*, 533−567.
13. Choudhury, J. R., and Bierbach, U. (2005) Characterization of the bisintercalative DNA binding mode of a bifunctional platinum-acridine agent, *Nucleic Acids Res. 33*, 5622−5632.
14. Jason, A. B., Karl, J. F., Shabana, A. S., Laura, L. W., and Jeffrey, T. P. (2002) Viscometry and atomic force microscopy studies of the interactions of a dimeric cyanine dye with DNA, *J. Phys. Chem. B 106*, 4838−4843.
15. Jose, M. P., Isabel, L.-S., Montero, E. I., Brana, M. F., Alonso, C., Robinson, S. P., and Navarro-Ranninger, C. (1999) Combined effect of platination and intercalation upon DNA binding of novel cytotoxic Pt-bis(naphthalimide) complexes, *J. Med. Chem. 42*, 5482−5486.
16. Bischoff, G., Bischoff, R., Birch-Hirschfeld, E., Gromann, U., Lindau, S., Meister, W. V., de, A. B. S., Bohley, C., and

Hoffmann, S. (1998) DNA-drug interaction measurements using surface plasmon resonance, *J. Biomol. Struct. Dyn. 16*, 187−203.
17. Modukuru, N. K., Snow, K. J., Perrin, B. S., Jr., Thota, J., and Kumar, C. V. (2005) Contributions of a long side chain to the binding affinity of an anthracene derivative to DNA, *J. Phys. Chem. 109*, 11810−11818.
18. Marchetti, S., Onori, G., and Cametti, C. (2005) DNA condensation induced by cationic surfactant: a viscosimetry and dynamic light scattering study, *J. Phys. Chem. 109*, 3676−3680.
19. Zang, H., and Gates, K. S. (2000) DNA binding and alkylation by the ”left half“ of azinomycin B, *Biochemistry 39*, 14968−14975.
20. Phillips, T., Haq, I., Meijer, A. J., Adams, H., Soutar, I., Swanson, L., Sykes, M. J., and Thomas, J. A. (2004) DNA binding of an organic dppz-based intercalator, *Biochemistry 43*, 13657−13665.
21. Scott, E. V., Jones, R. L., Banville, D. L., Zon, G., Marzilli, L. G., and Wilson, W. D. (1988) ^{1}H and ^{31}P NMR investigations of actinomycin D binding selectivity with oligodeoxyribonucleotides containing multiple adjacent d(GC) sites, *Biochemistry 27*, 915−923.
22. Baruah, H., and Bierbach, U. (2003) Unusual intercalation of acridin-9-ylthiourea into the 5′-GA/TC DNA base step from the minor groove: implications for the covalent DNA adduct profile of a novel platinum-intercalator conjugate, *Nucleic Acids Res 31*, 4138−4146.
23. Chaires, J. B. (1997) Energetics of drug-DNA interactions, *Biopolymers 44*, 201−215.
24. Kenji, T., Ryoji, K., Yoichi, T., Naohiko, S., and Kazuo, S. (2006) Formation of a DNA-including micelle by use of intercalation. *Polym. Preprints, Jpn. 55*, 1875.
25. Chiang, S. Y., Azizkhan, J. C., and Beerman, T. A. (1998) A comparison of DNA-binding drugs as inhibitors of E2F1- and Sp1-DNA complexes and associated gene expression, *Biochemistry 37*, 3109−3115.

BI602402M